Materials Chemistry and Physics 247 (2020) 122875

Contents lists available at ScienceDirect

Materials Chemistry and Physics

journal homepage: www.elsevier.com/locate/matchemphys

Metal-organic framework@polyaniline nanoarchitecture for improved fire safety and mechanical performance of epoxy resin

Shicong Ma [a], Yanbei Hou [a], Yuling Xiao [a], Fukai Chu [a], Tongmin Cai [b], Weizhao Hu [a,*], Yuan Hu [a,**]

[a] State Key Laboratory of Fire Science, University of Science and Technology of China, 96 Jinzhai Road, Hefei, Anhui, 230026, PR China
[b] KingFa Science and Technology Co. Ltd, Guangzhou, 510663, China

HIGHLIGHTS

- A Sn-based metal organic framework@polyaniline (Sn-MOF@PANI) was synthesized.
- When the loading was 2 wt%, EP/Sn-MOF@PANI showed good flame retardancy.
- Based on the analysis of the gaseous products and the condensed phase, a possible flame retarding mechanism was proposed.
- EP/Sn-MOF@ PANI had better mechanical properties than pure EP.

GRAPHICAL ABSTRACT

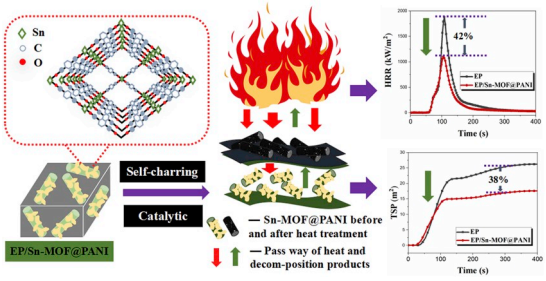

ARTICLE INFO

Keywords:
Metal organic frameworks
Smoke suppression
Flame retardancy
Mechanical property

ABSTRACT

In this work, a novel three-dimensional nanoarchitecture metal-organic framework@polyaniline (Sn-MOF@PANI) was designed and applied to address the fire hazards of epoxy resins (EP). Fourier transform infrared (FTIR), X-ray diffraction (XRD), X-ray photoelectron spectroscopy (XPS) and scanning electron microscopy (SEM) results proved that the Sn-MOF@PANI was successfully synthesized. Compared with pure EP, the peak heat release rate (PHRR) and the total heat release (THR) of EP/Sn-MOF@PANI were reduced by 42% and 32%, respectively. Meanwhile, the total smoke production (TSP) and total gaseous products of EP/Sn-MOF@PANI were also reduced during the combustion. The above results illustrate that the fire safety of EP was improved. Based on the analysis of the gaseous products and the condensed phase, a possible flame retarding mechanism was proposed. Moreover, the addition of Sn-MOF@PANI improved mechanical properties of EP, including storage modulus and impact strength.

1. Introduction

Epoxy resin (EP) has become one of the most important polymers because of its high mechanical properties, excellent bonding properties, low cure shrinkage and good process-ability. It also has strong adhesion, variable structure, high chemical stability and good corrosion resistance. It is widely used in multiple fields such as chemical industry, coating, semiconductor devices, etc. [1–4] However, the flammability of

* Corresponding author.
** Corresponding author.
E-mail addresses: hwz1988@ustc.edu.cn (W. Hu), yuanhu@ustc.edu.cn (Y. Hu).

https://doi.org/10.1016/j.matchemphys.2020.122875
Received 19 November 2019; Received in revised form 29 February 2020; Accepted 2 March 2020
Available online 5 March 2020
0254-0584/

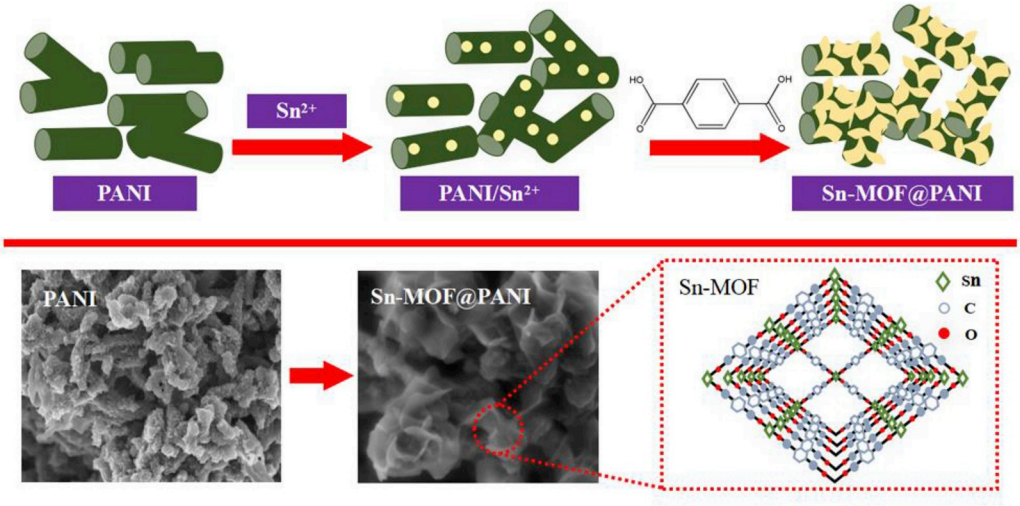

Scheme 1. Schematic illustration of preparation process of Sn-MOF@PANI hybrids.

EP limits its application, especially in areas where high flame retardancy is required, such as construction, chemicals, and electrical [5–7]. Therefore, more attention should be paid to improve the flame retardancy of EP. As ecological and environmental issues become more serious, halogen-free flame retardants have become a research hotpots and have gradually replaced traditional halogen-containing flame retardants [8,9].

According to the previous studies, polyaniline (PANI) can act as flame retardants for polymer materials. For example, there are experiments in which spherical PANI nanostructures are mixed as fillers into epoxy resin. The introduction of PANI not only reduces peak heat release rate (PHRR) value but also increases char residue of EP [10]. This is attributed to good self-charring ability of PANI [11]. In addition, the pectin/aniline flame retardant aerogel prepared by the polymerization-solidification method also exhibits good flame retardancy [12]. Furthermore, polyaniline can be used as a coupling agent to enhance inter-facial adhesion by forming covalent bonds between PANI and epoxy chains, thus improving the dispersion of nano-additives in EP [13,14]. The flame retardant effect of polyaniline is mainly reflected in the condensed phase, which can increase char residue to block the transmission of heat and gas.

Metal-organic frameworks (MOFs) are a new class of porous materials that have received extensive attention in recent years. They are coordination polymers formed by self-assembly of multidentate organic ligands with inorganic metal centers (metal ions or metal clusters) [15]. At present, the metal components are mainly transition metal ions and the ligands mainly based on carboxyl group or nitrogen-containing heterocyclic [16]. MOFs are gradually applied in the field of gas adsorption and separation [17], sensors [18], drug delivery [19], and catalytic reactions [20] for its large specific surface area and controllable pore structure. With the increasing variety of MOFs and the gradual rise of complex MOFs, they will have invaluable application prospects. In addition, its tunable physicochemical properties make it can be used as precursors or sacrificial templates for other functional materials [21]. Recently, there are some reports on the application of MOF in the field of flame retardants [22–24]. Zheng et al. prepared three different MOFs and added them to EP to study their thermal stability, flame retardancy and smoke suppression. The results showed that when the addition amount was 2%, the heat release rate (HRR) and the smoke production release (SPR) were reduced, and the char residue was increased [25]. Hou et al. synthesized Co-MOF and Fe-MOF by solvothermal method and added them to polystyrene (PS). When the loading was 2%, the HRR and SPR values of PS were all reduced, and the release of toxic styrene oligomers was suppressed [26]. During polymer combustion, the porous structure of MOF helps to adsorb volatile gases and macromolecules, thus reducing the release of toxic gases. Catalysis effect of metals is beneficial for the oxidation of toxic gases such as CO. In addition, MOF can promote the formation of a carbon layer, which can inhibit heat transfer and gas volatilization during combustion [27,28]. However, the dispersibility of MOF is generally poor, which easily led to the degradation of mechanical properties of materials [29].

Based on the above description, we envisioned a simplified protocol to fabricate PANI modified Sn-MOF (Sn-MOF@PANI) and investigated its synergistic effect on facilitating the flame retardant effect of polymer. All characterization results confirmed Sn-MOF, PANI rods and Sn-MOF@PANI hybrids were successfully synthesized and the additives were added to EP by physical blending. The flame retardancy of EP composites was investigated and it demonstrated that EP/Sn-MOF@PANI exhibited superior fire safety. Based on the analysis of the gaseous products and the char residue, a detailed flame retardant mechanism was proposed.

2. Experimental section

2.1. Preparation of Sn-MOF and Sn-MOF@PANI

To synthesize layered Sn-MOF, 0.48 g NaOH (0.012 mol) and 0.995 g terephthalic acid (0.006 mol) were dissolved in a 300 mL of deionized (DI) water under magnetic stirring, an aqueous solution in which 2.58 g of $SnSO_4$ (0.012 mol) dissolved was added to the above solution over 20 min. It was observed that white precipitate appeared rapidly after the addition of $SnSO_4$. The reaction temperature was raised to 90 °C and stirred for 1 h, then the reaction was continued for 5–6 h at room temperature. Finally, the solution was filtered and washed 3 times with deionized water to obtain Sn-MOF.

The synthesis of polyaniline (PANI) refers to the previous literature [30]. The preparation method of Sn-MOF @PANI was as shown in Scheme 1. The metal salt was dissolved in an aqueous solution of PANI and completely dispersed by ultra-sonication for 0.5 h, the following steps were similar to the preparation method of Sn-MOF. A dark green Sn-MOF@PANI powder was obtained by suction filtration and dried for use.

2.2. Preparation of EP and its composites

Take EP/Sn-MOF @ PANI as an example. First, 2.0 g of Sn-MOF @PANI hybrid was dispersed in 100 mL of acetone and sonicated for 0.5 h. Subsequently, 98.0 g of epoxy resin was poured into the above

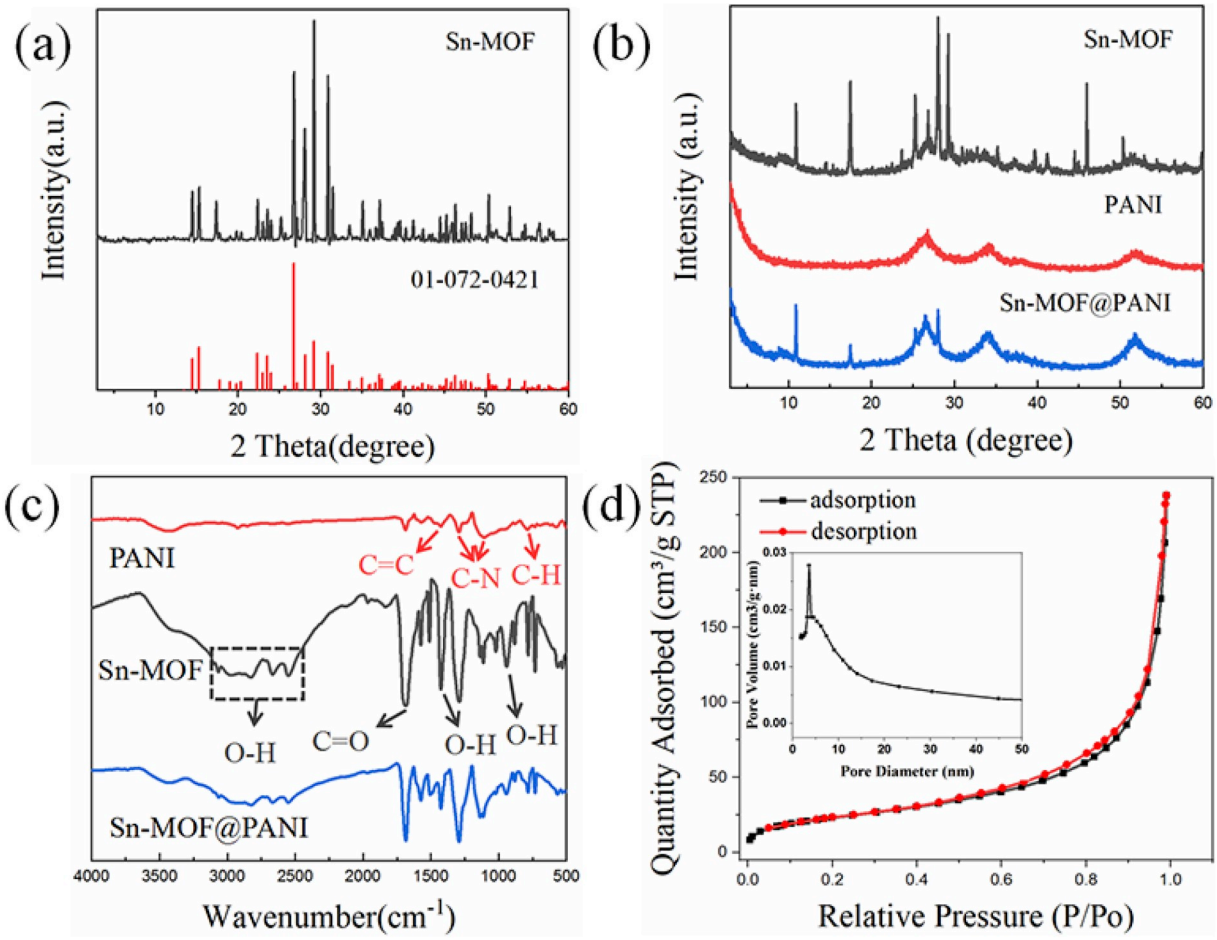

Fig. 1. XRD curves of Sn-MOF, PANI and Sn-MOF@PANI (a and b); FTIR spectra of Sn-MOF, PANI and Sn-MOF@PANI (c); N_2 adsorption−desorption isotherms and pore diameter distribution of Sn-MOF (d).

suspension and sonicated for another 0.5 h. The mixture was then heated at 100 °C for 6 h to remove the solvent. Finally, 21.78 g of liquid diaminodiphenyl-methane (DDM) was quickly added to the mixture with vigorous stirring. After stirring about 2 min, the mixture was poured into a mold and cured at 100 °C, 150 °C for 2 h. Other EP composites were prepared in the same procedure. In this work, the addition amount of the fillers were based on the total amount of the fillers and EP. Therefore, the loading of the fillers was 2 g/(2 g + 98 g) = 2%.

3. Results and discussion

3.1. Characterization of Sn-MOF and Sn-MOF@PANI

The crystal structure of the prepared compounds were characterized by powder X-ray diffraction (PXRD). Fig. 1a shows the PXRD profile of Sn-MOF and the well-defined diffraction peaks represent the high crystallinity of the sample [31,32]. Further, the diffraction peaks of Sn-MOF are similar to the Tritin (ii) dihydroxide sulfate [33], demonstrating that they have similar porous crystal structure. Generally, the characteristic peaks of PANI appear at 15°, 20.5°, and 26°, which correspond to the (011), (020), and (200) crystal planes, respectively [34]. The broad peak at 26° in Fig. 1b indicates that PANI is amorphous. The characteristic peaks of single compound appear in the XRD curve of Sn-MOF@PANI, declaring that its crystal state has not changed during the hybridization process.

In order to deeply analyze the molecular structure of the compounds, FTIR spectrum was performed and shown in Fig. 1c. The characteristic absorption peaks of Sn-MOF can be observed at 2500 to 3200, 1680, 1400, 920, and 750 cm^{-1}, which are mainly derived from the vibration of carboxylate groups [35]. The broad peaks of 2500–3200 cm^{-1} and several small peaks around 2700 cm^{-1} correspond to tensile vibration and deformation vibration of the O–H bond [36]. The absorption peaks at 1680 and 1411 cm^{-1} are attributed to the stretching vibration of C═O and O–H of the carboxylic acid. The bending vibration peak of O–H is at 920 cm^{-1}, and the peak at 750 cm^{-1} corresponds to the C–H bending vibration of benzene [37]. In the spectrum of PANI, the peak at 1480 cm^{-1} is related to the stretching vibration of C═C bond, the peaks at 1296 and 1112 cm^{-1} are attributed to the C–N stretching vibration of the benzenoid unit and quinoid rings in PANI. The adsorption peaks at 1230 and 780/730 cm^{-1} are attributed to the stretching vibration and out of plane vibration of the C–H bond, respectively. The characteristic adsorption peaks of Sn-MOF and PANI can be detected in the spectrum of Sn-MOF@PANI, indicating that Sn-MOF nanosheets have been successfully grown on the PANI rods.

Sn-MOF was investigated by Brunauer -Emmett-Teller (BET) test to reveal its porous structure. It can be seen from Fig. 1d that the adsorption isotherm of the sample can be classified as type IV of IUPAC classification (type IV is characterized as a strong affinity mesoporous adsorbent. At lower temperatures, they show adsorption hysteresis) [38]. The nitrogen adsorption-desorption isotherm of Sn-MOF shows H3-type hysteresis, which indicates that there are slits formed by the accumulation of flake particles [39]. The pore size distribution curve is displayed in Fig. 1d and it consists of a peak at 2–4 nm and a broad peak at 10–30 nm, confirming the presence of micropores and mesopores in the Sn-MOF. The specific surface area of Sn-MOF is 79.9 $m^2\ g^{-1}$, which is

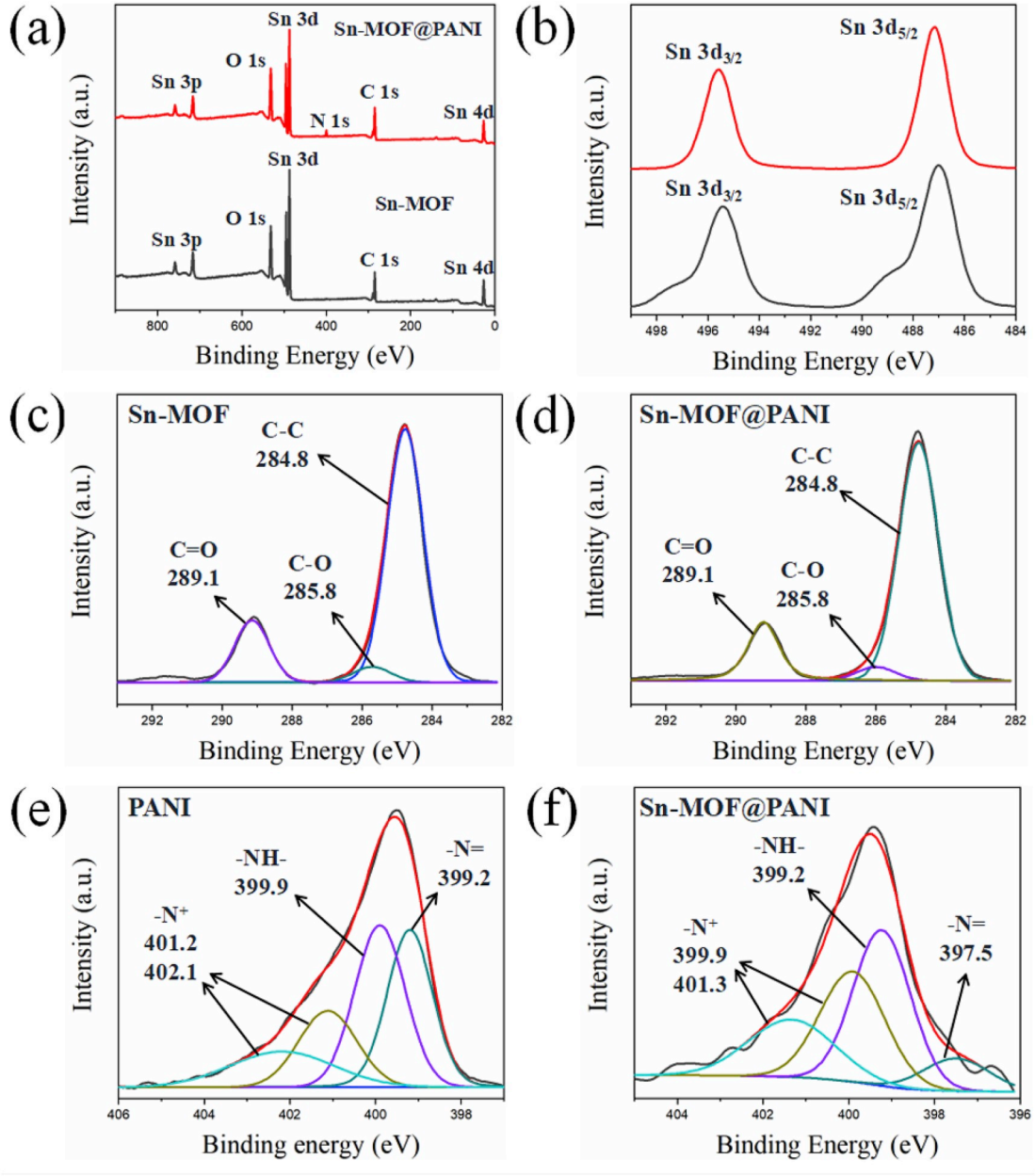

Fig. 2. XPS curves of Sn-MOF, PANI and Sn-MOF@PANI.

much larger than the previous literature. It has been previously reported that the specific surface area of the synthesized Sn-MOF is less than 15 $m^2 g^{-1}$ [40,41]. It can be seen from Fig. S1 that the type of the nitrogen adsorption-desorption isotherm of Sn-MOF@PANI is the same as that of Sn-MOF and its specific surface area is 55.1 $m^2 g^{-1}$. The porous structure facilitates the absorption of gaseous products during polymer pyrolysis, thereby delaying the transport of gases from the interior space to the combustion zone. On the other hand, a larger specific surface area provides more catalytic sites for metal compounds [42].

XPS is used to detect the chemical state of Sn-MOF, PANI and Sn-MOF@PANI and the XPS spectrum of Sn is shown in Fig. 2b. The Sn 3d spectra in Sn-MOF show two binding energy peaks at 487.3 eV and 497.2 eV, corresponding to Sn $3d_{3/2}$ and Sn $3d_{5/2}$, respectively [43]. In contrast, the fitting peak of the Sn element in Sn-MOF @ PANI shifted to a high binding energy, indicating that it lost electrons during the charge transfer process, and some Sn^{2+} was oxidized to Sn^{4+} [44]. In Fig. 2c, the C 1s XPS spectrum shows a main peak of 284.8 eV followed by two lower intensity peaks, caused by sp2 hybridized carbon. The peak at 285.8 eV is attributed to the C–O produced by the sp3 hybrid carbon, the peak of 289.1 eV is the C═O of the carbonyl group and the carboxylate [45].The N1s spectrum of PANI contains four main peaks (398.2, 399.0, 401.2 and 402.1 eV) (as shown in Fig. 2e), corresponding to quinone imine (N), anilide (NH), positively charged imine (bipolarized state) and protonated amine (polarized state), respectively [46]. The binding energy of N 1s in the hybrid moves toward low value, confirming that the electrons are acquired by the nitrogen during charge transfer process [47]. The above results indicate that an interaction occurs between the metal site and the aniline unit during the compounding process. Furthermore, it can be calculated from Table S1 that the contents of Sn-MOF and PANI in the hybrids are 68.9% and 31.1%, respectively.

The microstructure of the compounds were characterized by scanning electron microscopy (SEM). It should be stated that the samples were dispersed in ethanol solvent before taking SEM images. As shown in Fig. 3a, Sn-MOF shows good dispersion state, indicating that it can be dispersed uniformly in solvent. Furthermore, a layered structure can be observed from the enlarged image. EDS test was used to analyze

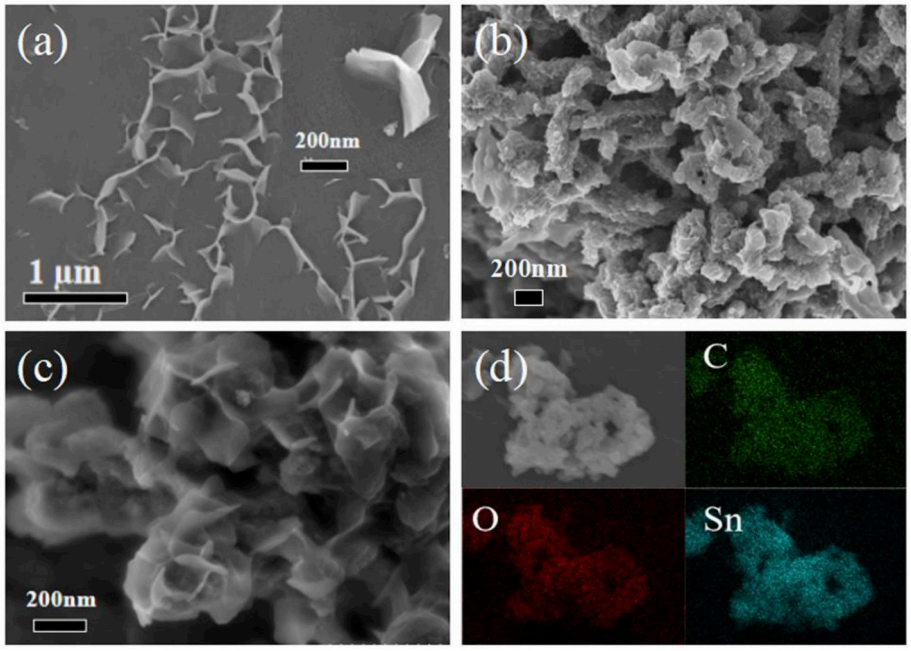

Fig. 3. SEM images of Sn-MOF (a), PANI (b) and Sn-MOF@PANI (c); SEM image of Sn-MOF@PANI with mapping mode (d).

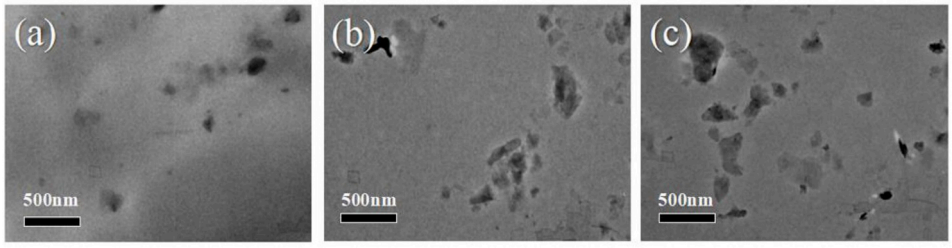

Fig. 4. TEM images of the sliced surface of the EP composite (a) EP/Sn-MOF, (b) EP/PANI, (c) EP/Sn-MOF@PANI.

elemental composition of Sn-MOF. It can be seen that C, O and Sn elements are detected from Fig. S2, which indicates that the composition of Sn-MOF is consistent with the design. It should be noted that Cu and Au elements are derived from copper support and conductive gold. The structure of PANI in Fig. 3b is short rod shape, which is consistent with the amorphous morphology reported in the literature [48]. Fig. 3c is an enlarged image of Sn-MOF@PANI. It can be observed that Sn-MOF nanosheets grow uniformly on the surface of PANI. The EDS mapping image of Sn-MOF@PANI (Fig. 3d) shows that the elements are evenly distributed according to the shape of the composites, thus confirming the successful synthesis of the compound.

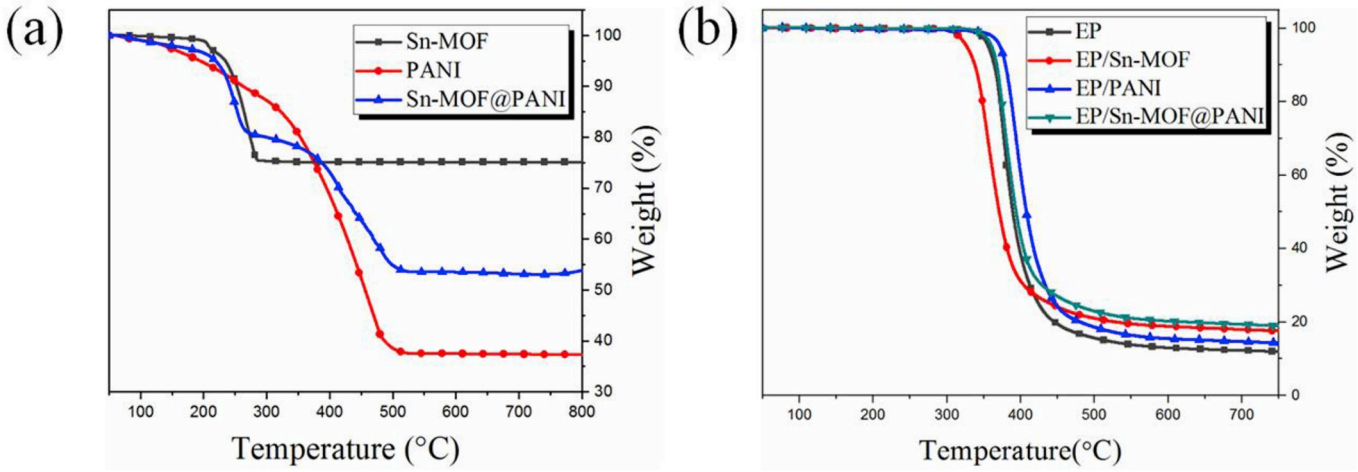

Fig. 5. TGA curves of the fillers (a) and EP composites (b) under N_2 conditions.

Table 1
TGA data of the pure EP, EP/Sn-MOF, EP/PANI and EP/Sn-MOF@PANI.

Sample	N_2		
	T_i[a]	T_{max}[b]	W_{800}(%)[c]
EP	364.0	374.9	10.6
EP/Sn-MOF	337.0	353.1	17.3
EP/PANI	379.3	395.4	14.2
EP/Sn-MOF@PANI	367.2	379.3	19.5

[a] The temperature where 10 wt% of weight was lost.
[b] The temperature where the maximum weight loss occurred.
[c] The residual weight at 800 °C.

3.2. Dispersion state of fillers in EP

The fractured surfaces of EP and its composites were observed by SEM to study the influence of the additives on the micro-topographies. From Fig. S3a, pure EP exhibits a typical brittle fracture microstructure with cracks. The fractured structures can be clearly observed in the enlarged image (Fig. S3e). As shown in Figs. S3b and c, EP/Sn-MOF and EP/PANI show rough surface and the enlarged images show irregular fracture layer (Figs. S3f and g). It can be seen from Fig. S3d that the fracture surface of EP/Sn-MOF @PANI has no obvious protrusions, and is flatter than EP/Sn-MOF and EP/PANI. In the magnified view (Fig. S3h), EP/Sn-MOF@PANI has no obvious chasm phenomenon and debris. The possible reason is that PANI can act as a coupling agent to improve the dispersion state of Sn-MOF in EP [12].

In order to further study the dispersion state of nanofillers in EP, the images of ultra-thin sections of EP composites were observed by transmission electron microscopy (TEM), as shown in Fig. 4. As can be seen from Fig. 4a, there are irregular spots and 'shadows' due to the agglomeration of Sn-MOF in the matrix. 'Shadows' are bumps and depressions on the surface of a material, which are caused by agglomeration of additives. It can be seen from Fig. 4b and c that the images of EP/PANI and EP/Sn-MOF@PANI have agglomeration but no 'shadows'. The above results indicate that the presence of PANI can improve the interaction between the nanofillers and the matrix, thus improving the compatibility [13].

3.3. Thermal stability of EP and its composites

The thermal oxidation behavior of the additive was analyzed by TGA equipment and the results are shown in Fig. 5a. In the initial stage (<200 °C), all of samples show good thermal stability. PANI decomposes faster after 350 °C, mainly due to the degradation of its skeleton [11]. The decomposition of Sn-MOF at 200–300 °C is mainly attributed to the release of ligands in the pores of the metal skeleton [49]. Sn-MOF@PANI shows the thermal decomposition behavior of single component. After heat treatment at 800 °C, the char residue of Sn-MOF, PANI and Sn-MOF@PANI is 75.1%, 37.3% and 53.9%, respectively.

Fig. 5b shows the TG curves of different composites and Table 1 gives the relevant data. It can be found that T_i and T_{max} of pure EP are 364.0 °C and 374.9 °C, respectively. While the T_i and T_{max} of EP/Sn-MOF composites decreased to 337.0 °C and 353.1 °C, which was mainly due to the catalytic degradation of Sn-MOF [41]. However, due to the excellent thermal stability of PANI, the T_i and T_{max} of EP/PANI composites increased to 379.3 °C and 395.4 °C, respectively. In addition, it can be observed that the char yield of EP/Sn-MOF@PANI is highest at 700 °C, indicating that Sn-MOF and PANI have a synergistic effect in promoting char formation.

3.4. Combustion behaviors

Cone calorimetry is a widely used method for assessing the combustion properties of materials [50]. The combustion performance of the material was quantitatively analyzed by studying parameters such as heat release rate, smoke production release and toxic gas (CO) release rate [51]. It can be seen from Fig. 6a and d that the HRR of pure EP increases rapidly during the combustion, with a PHRR value of 1879 kW m^{-2}. The addition of additives can reduce PHRR and THR of EP. Under the same loading, the PHRR value of EP/Sn-MOF is higher than EP/PANI while the THR value is lower, indicating that the catalytic char formation of Sn-MOF effectively improves the barrier effect of the carbon layer. The addition of Sn-MOF@PANI can significantly reduce PHRR and THR (reduced by 42% and 32%, respectively), which is better than single component. It demonstrated that the synergy effect can improve the fire safety of EP composites. Furthermore, it is worth noting that the reduction of PHRR and THR of EP/Sn-MOF @ PANI is better than

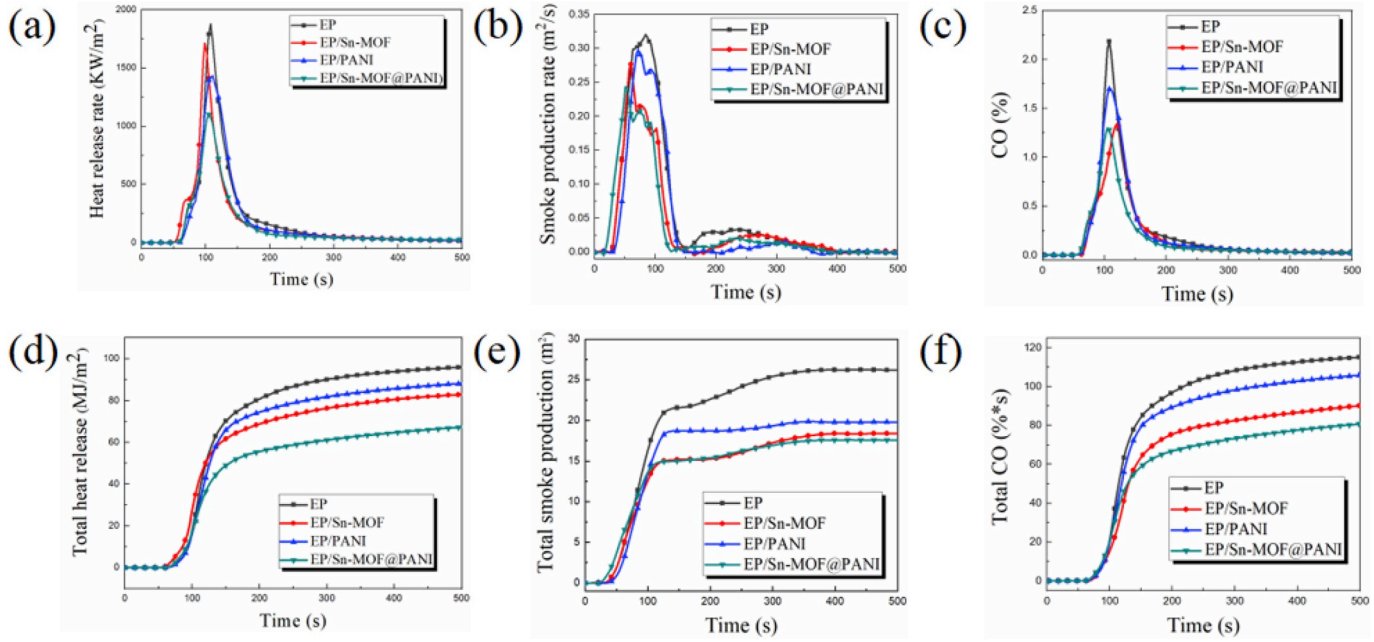

Fig. 6. Heat release rate (HRR) (a), Smoke production rate (SPR) (b), CO release (c), Total heat release (THR) (d), Total smoke production (TSP) (e), and total CO release (f) curves of EP and its assemble systems.

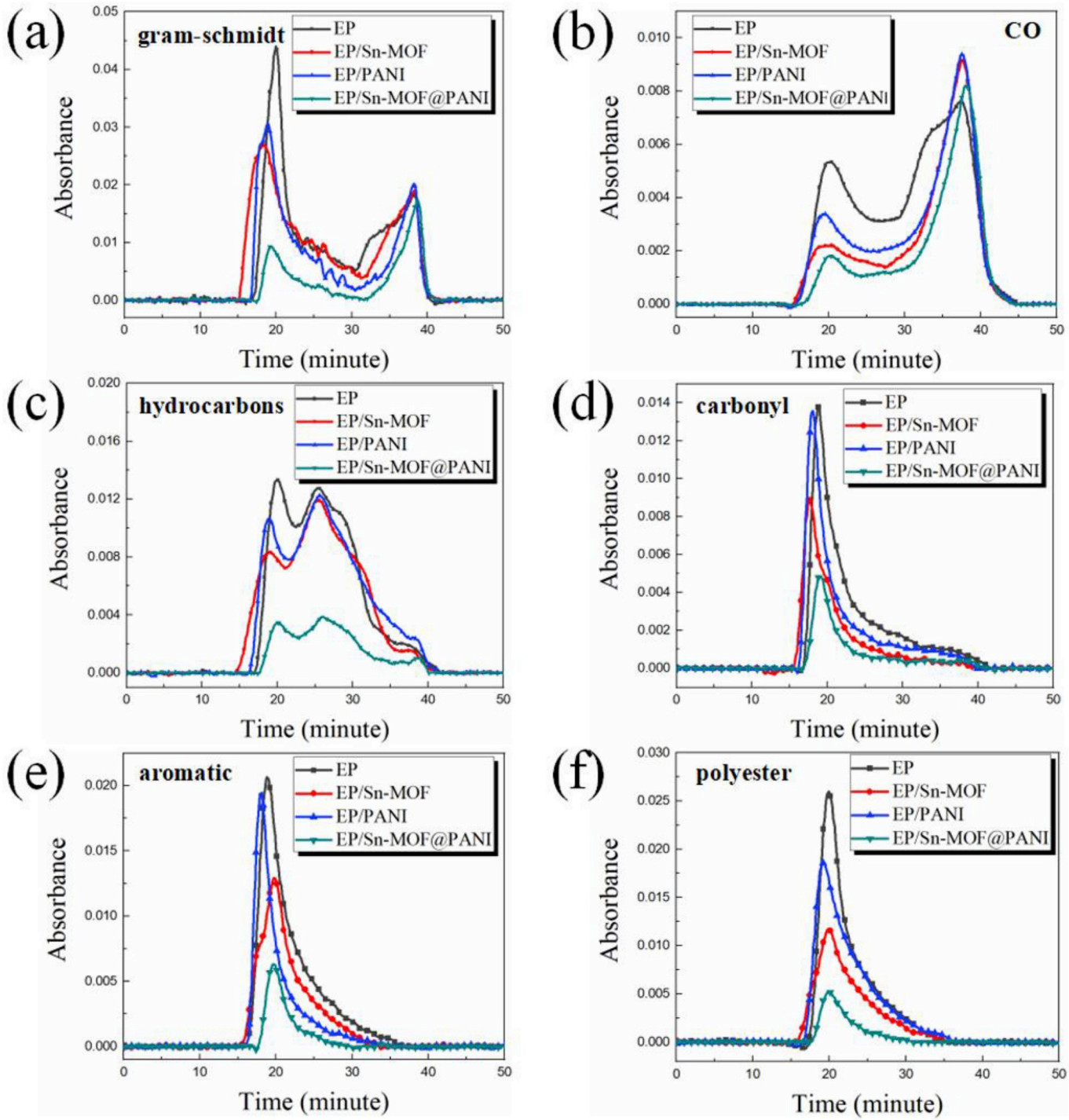

Fig. 7. Intensities of characteristic peaks of Gram−Schmidt (a), CO release curves (b), carbonyl compounds (c), aliphatic polyester (d), hydrocarbons (e), and aromatic compounds (f) of EP and its assembled systems.

previous literature [11,13,14].

The smoke release behavior of polymers is another important indicator for evaluating fire safety of polymers. As shown in Fig. 6b and e, smoke production rate (SPR) and total smoke production (TSP) are reduced. It is clear that the additives have good performance in reducing smoke release and Sn-MOF@PANI has the best efficiency on smoke suppression. The peak smoke production rate (PSPR) and TSP of EP/Sn-MOF@PANI decreased by 38% and 33%. Compared with the previous EP nanocomposites, EP/Sn-MOF @ PANI has better effect in reducing the PSPR and TSP [52–54]. Fig. 6c and f confirm the superiority of Sn-MOF on reducing CO generation. PANI can slightly reduce the overall CO yield while the total CO yield of EP/Sn-MOF and EP/Sn-MOF @PANI is reduced by 23% and 31%, respectively. The above results declare that the additives have good smoke suppressing efficiency.

3.5. *Analysis of evolved gases*

The addition of flame retardant generally reduces the release of flammable gases, thereby inhibiting the combustion process of the polymer matrix. In order to understand the thermal decomposition

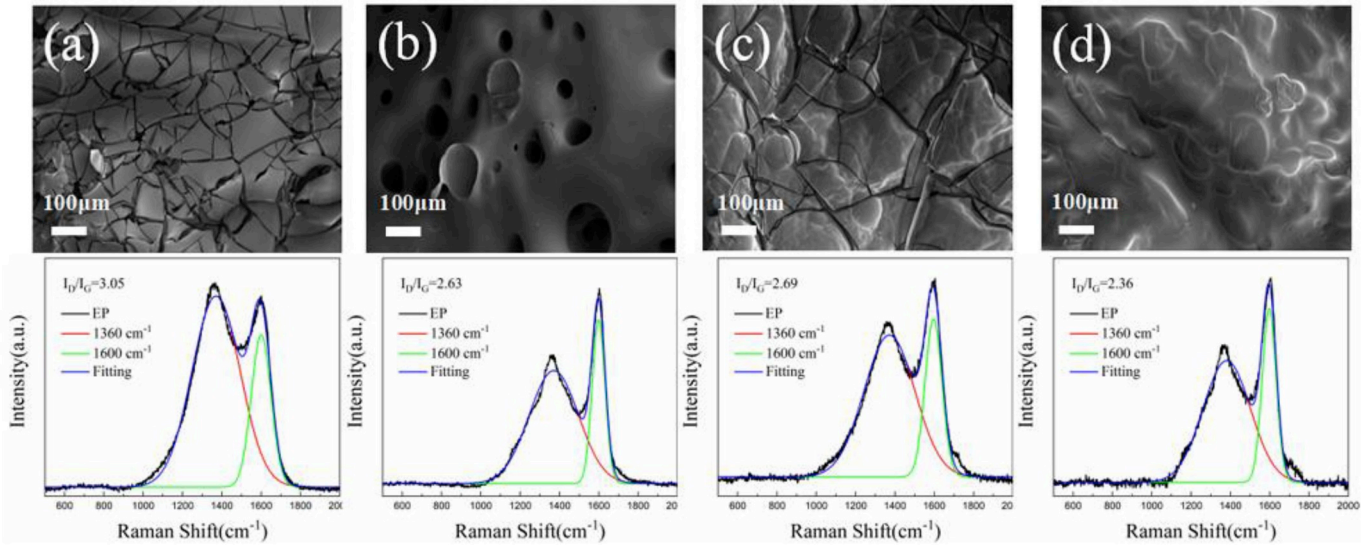

Fig. 8. SEM images and corresponding Raman spectra of char residues of (a) EP, (b) EP/Sn-MOF, (c) EP/PANI, and (d) EP/Sn-MOF@PANI.

mechanism of the hybrids, the evolution of the pyrolysis gas was detected by TG-IR technique. The time evolution of the total gaseous product is shown in Fig. 7a. It can be seen that the addition of single component has little effect on the overall yield of gaseous products, but it can significantly reduce the peak total gaseous release (38.6% and 31.5%, respectively). It is worth noting that the addition of Sn-MOF@PANI not only reduces the overall production of gaseous products (about 66.7%) but also delays the time to peak total gaseous release. It will save precious time for escaping and disaster relief when a real fire accident occurs. Of course, this again confirms the synergistic effect between PANI and Sn-MOF.

Figure S4a is the FTIR spectra of EP and its composites at 19.2 min. All samples show similar curves, consisting of characteristic bands such as –OH (3653 cm^{-1}), –CH groups (2800-3100 cm^{-1}), aromatic compounds (1608, 1512, 830 and 743 cm^{-1}), carbonyl compounds (1740 cm^{-1}) and polyesters (1253 and 1175 cm^{-1}) [55]. It can be seen that the peak intensity is weakened or even unrecognized after adding additives, indicating that the release of volatile organic compounds is significantly inhibited. On the other hand, it is clearly that the addition of additives can suppress the release of CO. Among the toxic gases produced by combustion, carbon dioxide mainly increases the breathing and ventilation rate of people, resulting in an increase in the inhalation of other toxic gases [56]. The additives can reduce the release of carbon dioxide (Fig. S4b), further enhancing the probability of people's escape in a fire accident.

To further understand the suppression effect of nanofillers on the release of volatiles, the time-dependent release curves of pyrolysis products (including hydrocarbons, carbonyl compounds, aromatics and aliphatic polyesters) are shown in Fig. 7. It can be seen that the addition of nanofillers can inhibit the release of the above-mentioned organic products and the inhibition efficiency of Sn-MOF@PANI is the best. The reduction in organic groups is beneficial to the suppression of smoke

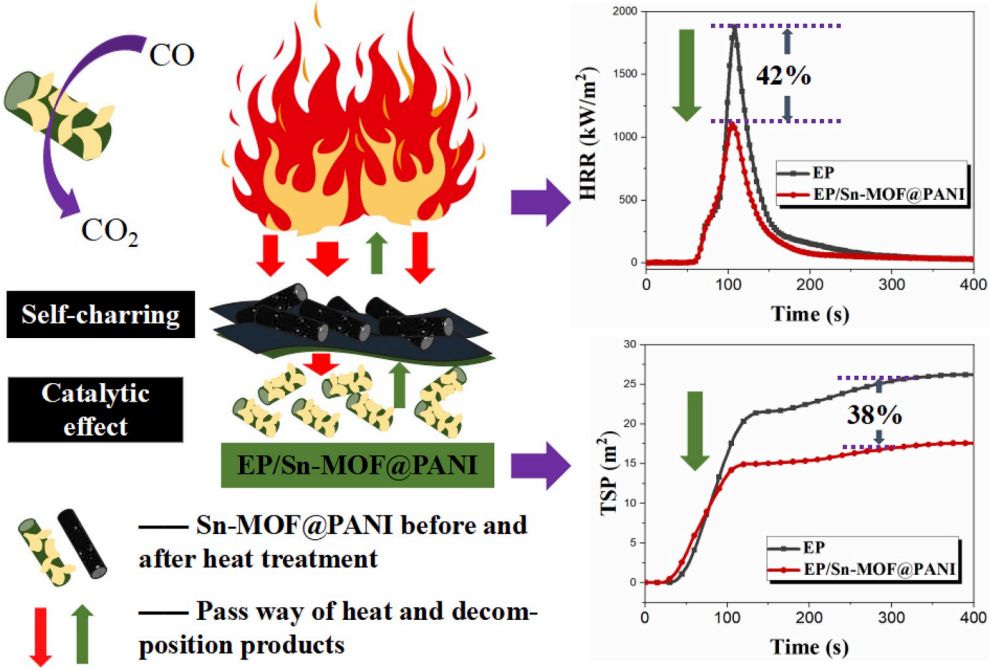

Scheme 2. Schematic illustration for the mechanisms of flame retardancy.

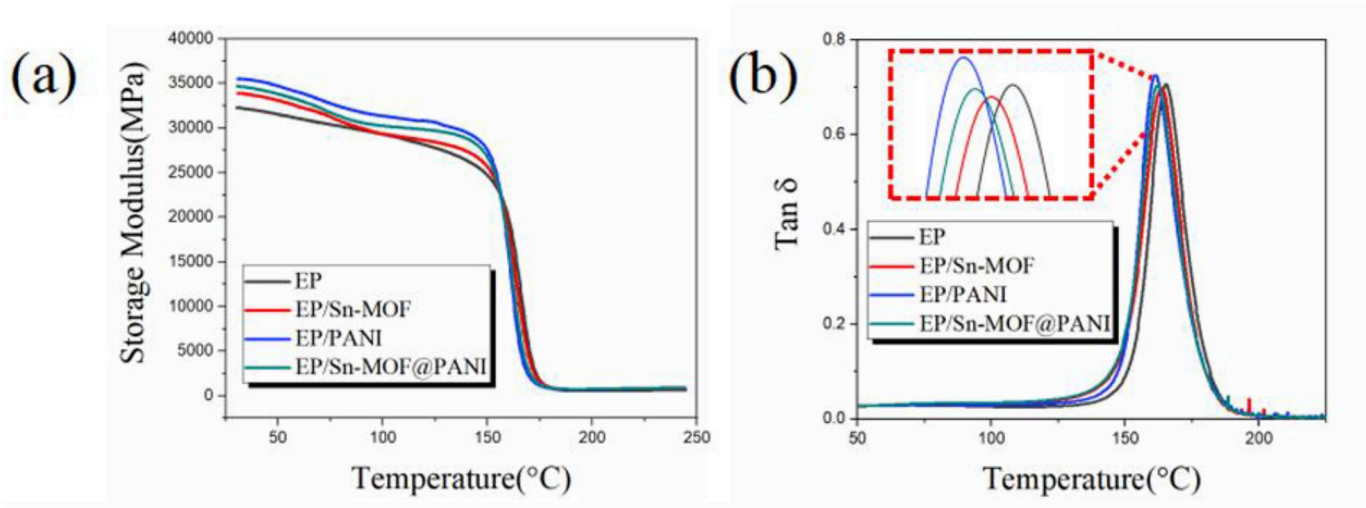

Fig. 9. Storage modulus (a) and Tan δ curves (b) of EP and its composites.

emission, as these organic compounds can aggregate to form smoke particles after cooling. Moreover, the reduced organic compound may migrate and form char residues in the condensed phase [57]. As evidenced by the increased char yield in the TGA results.

3.6. Analysis of char residues

The properties of char residue, including weight, degree of graphitization and micromorphology have been widely used to analyze the flame retardant mechanism of additives. As shown in Fig. 8, many cracks and caves can be observed from the char residue of pure EP, and the carbon layer showed no signs of swelling. The carbonization process has been improved after adding additives and a continuous and expanded carbon layer appears in the view. The D and G bands at 1360 and 1600 cm^{-1} correspond to the vibration of carbon from disordered carbon-containing compounds and graphite-containing compounds, respectively [58]. The integrated intensity ratio of the D and G bands (I_D/I_G) is used to evaluate the degree of graphitization. The highly graphitized char layer can fully exert a barrier effect to suppress the transfer of heat and volatile gases, thereby improving flame retardancy of polymeric composites. It can be seen from Fig. 8 that EP has the highest I_D/I_G value and EP/Sn-MOF@PANI has the lowest. The above results indicate that the char residue produced by EP/Sn-MOF@PANI has a high degree of graphitization and its shows better efficiency in preventing heat transfer and the spread of flame.

On the basis of the above analysis, the possible flame retardant mechanism of Sn-MOF @ PANI is described and the schematic illustration is shown in Scheme 2. EP composites release a large amount of volatile compounds and gradually form a carbon layer as the combustion progresses. The self-charring ability of polyaniline can improve the yield of char residue and the formation of carbon layer can suppress the transfer of gas and heat [12]. On the other hand, Sn-MOF can absorb volatile gases due to its large specific surface area, thereby reducing the release of flammable gases. Furthermore, Sn-MOF can increase the graphitization degree of the carbon layer to improve the barrier efficiency. Simultaneously, Sn-MOF can produce SnO_2 during the combustion process, which can catalyze the oxidation of CO, thus reducing the concentration of toxic gases [59,60].

3.7. Mechanical analysis

The viscoelastic properties of EP and its composites were evaluated by dynamic mechanical thermal analysis. The storage modulus E′ and the loss factor tan δ curves are shown in Fig. 9. It can be seen that all

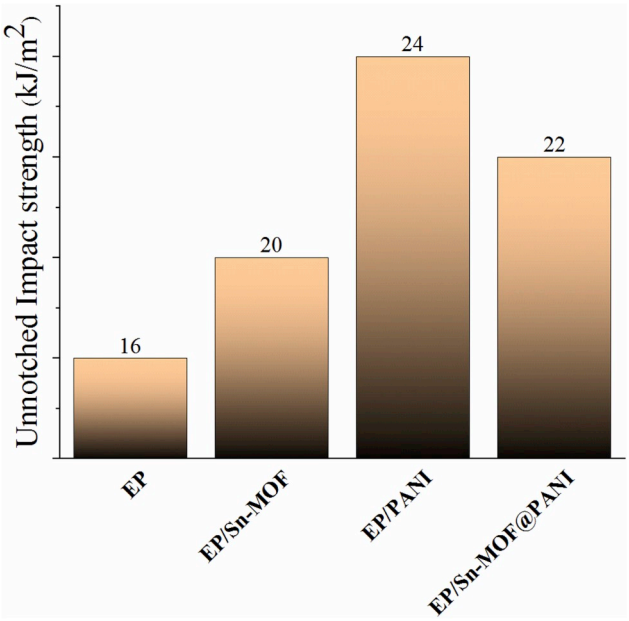

Fig. 10. Non-notched impact strength of EP and its composites.

samples show the typical viscoelastic behavior of thermoset polymers, transitioning from a glass platform to a rubber platform [61]. For thermoset nanocomposites, the storage modulus mainly depends on the inorganic phase, interfacial interaction and the crosslink density of the polymer matrix. The storage modulus of epoxy composites in the glass plateau is higher than pure epoxy resin. It is primarily due to the addition of nanofillers enhances the interfacial interaction between the epoxy resins, thereby reducing the flow of the epoxy matrix around the additives [62].

The glass transition temperature (T_g) of EP and its composites is shown in Fig. 9b. It can be found that all the loss factor curves show only one transition peak, indicating that the additives has good compatibility with EP [63]. In addition, the T_g value of EP composites decreased slightly compared to pure EP, which may be attribute to the reduction of crosslinking density in the modified sample.

The mechanical properties of EP composites were evaluated by cantilever beam impact testing machine and non-notched impact strength is shown in Fig. 10. The impact strength of EP composites has been improved compared with pure EP, which is mainly because the

additives have a large specific surface area and a high absorption capacity for impact energy. Previous analysis showed that compared with Sn-MOF, PANI has better dispersibility in EP, and it can be used as reinforcing particles to enhance the strength of the matrix. Therefore, the notched impact strength of EP/PANI is better than EP/Sn-MOF and EP/Sn-MOF @PANI [61].

4. Conclusion

In this work, a novel metal-organic framework@polyaniline nanoarchitecture was successfully prepared. Sn-MOF grows on PANI nanorods, and the channels formed by the Sn-MOF sheet increase the pore volume and specific surface area of the hybrid, which is conducive to adsorption of gaseous products and macromolecules. The barrier effect of Sn-MOF and the char-formation property of PANI can block the transfer of heat and gases during combustion. Furthermore, EP/Sn-MOF@PANI had better mechanical performance than pure EP, including storage modulus and impact strength. This work showed the broad application prospect of MOFs in the field of flame retardant. On the other hand, it provided a design strategy to improve the compatibility of MOF and matrix, aiming at enhancing fire safety and improving mechanical properties.

Declaration of competing interest

The authors declare that they have no known competing financial interests or personal relationships that could have appeared to influence the work reported in this paper.

CRediT authorship contribution statement

Shicong Ma: Writing - original draft, Conceptualization, Data curation. **Yanbei Hou:** Writing - review & editing. **Yuling Xiao:** Software, Validation. **Fukai Chu:** Methodology. **Tongmin Cai:** Investigation. **Weizhao Hu:** Supervision, Writing - review & editing. **Yuan Hu:** Supervision.

Acknowledgement

The research was financially supported by the National Natural Science Foundation of China (No. 51874266, 51991352) and Fundamental Research Funds for the Central Universities (WK2320000041).

Appendix A. Supplementary data

Supplementary data to this article can be found online at https://doi.org/10.1016/j.matchemphys.2020.122875.

References

[1] X. He, W. Zhang, R. Yang, The characterization of DOPO/MMT nanocompound and its effect on flame retardancy of epoxy resin, Compos. Part. A-Appl. S. 98 (2017) 124–135.
[2] Q. Guan, L. Yuan, Y. Zhang, A. Gu, G. Liang, Improving the mechanical, thermal, dielectric and flame retardancy properties of cyanate ester with the encapsulated epoxy resin-penetrated aligned carbon nanotube bundle, Compos. B Eng. 123 (2017) 81–91.
[3] M.-J. Chen, X. Wang, X.-L. Li, X.-Y. Liu, L. Zhong, H.-Z. Wang, Z.-G. Liu, The synergistic effect of cuprous oxide on an intumescent flame-retardant epoxy resin system, RSC Adv. 7 (2017) 35619–35628.
[4] W. Cai, X. Feng, B. Wang, W. Hu, B. Yuan, N. Hong, Y. Hu, A novel strategy to simultaneously electrochemically prepare and functionalize graphene with a multifunctional flame retardant, Chem. Eng. J. 316 (2017) 514–524.
[5] R. Jian, P. Wang, L. Xia, X. Yu, X. Zheng, Z. Shao, Low-flammability epoxy resins with improved mechanical properties using a Lewis base based on phosphaphenanthrene and 2-aminothiazole, J. Mater. Sci. 52 (2017) 9907–9921.
[6] T. Ma, C. Guo, Synergistic effect between melamine cyanurate and a novel flame retardant curing agent containing a caged bicyclic phosphate on flame retardancy and thermal behavior of epoxy resins, J. Anal. Appl. Pyrol. 124 (2017) 239–246.
[7] R. Jian, P. Wang, W. Duan, J. Wang, X. Zheng, J. Weng, Synthesis of a novel P/N/S-containing flame retardant and its application in epoxy resin: thermal property, flame retardance, and pyrolysis behavior, Ind. Eng. Chem. Res. 55 (2016) 11520–11527.
[8] Z.B. Shao, C. Deng, Y. Tan, M.J. Chen, L. Chen, Y.Z. Wang, An efficient monocomponent polymeric intumescent flame retardant for polypropylene: preparation and application, ACS Appl. Mater. Interfaces 6 (2014) 7363–7370.
[9] C. Ma, S. Qiu, B. Yu, J. Wang, C. Wang, W. Zeng, Y. Hu, Economical and environment-friendly synthesis of a novel hyperbranched poly (aminomethylphosphine oxide-amine) as co-curing agent for simultaneous improvement of fire safety, glass transition temperature and toughness of epoxy resins, Chem. Eng. J. 322 (2017) 618–631.
[10] X. Zhang, Q. He, H. Gu, H.A. Colorado, S. Wei, Z. Guo, Flame-retardant electrical conductive nanopolymers based on bisphenol F epoxy resin reinforced with nano polyanilines, ACS Appl. Mater. Interfaces 5 (2013) 898–910.
[11] K. Zhou, C. Liu, R. Gao, Polyaniline: A novel bridge to reduce the fire hazards of epoxy composites, Compos. Part. A-Appl. S. 112 (2018) 432–443.
[12] H.-B. Zhao, M. Chen, H.-B. Chen, Thermally insulating and flame-retardant polyaniline/pectin aerogels, ACS Sustain. Chem. Eng. 5 (2017) 7012–7019.
[13] X. Zhang, Q. He, H. Gu, S. Wei, Z. Guo, Polyaniline stabilized barium titanate nanoparticles reinforced epoxy nanocomposites with high dielectric permittivity and reduced flammability, J. Mater. Chem. C. 1 (2013).
[14] H. Gu, J. Guo, Q. He, S. Tadakamalla, X. Zhang, X. Yan, Y. Huang, H.A. Colorado, S. Wei, Z. Guo, Flame-retardant epoxy resin nanocomposites reinforced with polyaniline-stabilized silica nanoparticles, Ind. Eng. Chem. Res. 52 (2013) 7718–7728.
[15] S. Dang, Q.-L. Zhu, Q. Xu, Nanomaterials derived from metal–organic frameworks, Nat. Rev. Mater. 3 (2017).
[16] L.J. Murray, M. Dinca, J.R. Long, Hydrogen storage in metal-organic frameworks, Chem. Soc. Rev. 38 (2009) 1294–1314.
[17] J.-R. Li, Y. Ma, M.C. McCarthy, J. Sculley, J. Yu, H.-K. Jeong, P.B. Balbuena, H.-C. Zhou, Carbon dioxide capture-related gas adsorption and separation in metal-organic frameworks, Coord. Chem. Rev. 255 (2011) 1791–1823.
[18] L.E. Kreno, K. Leong, O.K. Farha, M. Allendorf, R.P. Van Duyne, J.T. Hupp, Metal-organic framework materials as chemical sensors, Chem. Rev. 112 (2012) 1105–1125.
[19] P. Horcajada, C. Serre, M. Vallet-Regi, M. Sebban, F. Taulelle, G. Ferey, Metal-organic frameworks as efficient materials for drug delivery, Angew Chem. Int. Ed. Engl. 45 (2006) 5974–5978.
[20] C.-C. Wang, J.-R. Li, X.-L. Lv, Y.-Q. Zhang, G. Guo, Photocatalytic organic pollutants degradation in metal–organic frameworks, Energy Environ. Sci. 7 (2014) 2831–2867.
[21] X. Cao, C. Tan, M. Sindoro, H. Zhang, Hybrid micro-/nano-structures derived from metal-organic frameworks: preparation and applications in energy storage and conversion, Chem. Soc. Rev. 46 (2017) 2660–2677.
[22] Y. Hou, W. Hu, Z. Gui, Y. Hu, A novel Co(II)–based metal-organic framework with phosphorus-containing structure: build for enhancing fire safety of epoxy, Compos. Sci. Technol. 152 (2017) 231–242.
[23] Z. Sun, Y. Hou, Y. Hu, W. Hu, Effect of additive phosphorus-nitrogen containing flame retardant on char formation and flame retardancy of epoxy resin, Mater. Chem. Phys. 214 (2018) 154–164.
[24] Y. Hou, Y. Hu, S. Qiu, L. Liu, W. Xing, W. Hu, Bi2Se3 decorated recyclable liquid-exfoliated MoS2 nanosheets: towards suppress smoke emission and improve mechanical properties of epoxy resin, J. Hazard Mater. 364 (2019) 720–732.
[25] Y. Zheng, Y. Lu, K. Zhou, A novel exploration of metal-organic frameworks in flame-retardant epoxy composites, J. Therm. Anal. Calorim. 138 (2019) 905–914.
[26] Y. Hou, W. Hu, Z. Gui, Y. Hu, Preparation of metal-organic frameworks and their application as flame retardants for polystyrene, Ind. Eng. Chem. Res. 56 (2017) 2036–2045.
[27] R. Semino, J.C. Moreton, N.A. Ramsahye, S.M. Cohen, G. Maurin, Understanding the origins of metal-organic framework/polymer compatibility, Chem. Sci. 9 (2018) 315–324.
[28] Y. Hou, L. Liu, S. Qiu, X. Zhou, Z. Gui, Y. Hu, DOPO-modified two-dimensional Co-based metal-organic framework: preparation and application for enhancing fire safety of poly(lactic acid), ACS Appl. Mater. Interfaces 10 (2018) 8274–8286.
[29] Y. Hou, W. Hu, Y. Hu, Preparation of layered organic-inorganic aluminum phosphonate for enhancing fire safety of polystyrene, Mater. Chem. Phys. 196 (2017) 109–117.
[30] S. Pandey, S. Annapoorni, B.J.M. Malhotra, Synthesis and characterization of poly (aniline-co-o-anisidine), A processable conducting copolymer 26 (1993) 3190–3193.
[31] C.-C. Lin, J.-M. Ho, H.-L. Hsieh, Feasibility of using a rotating packed bed in preparing Fe3O4 nanoparticles, Chem. Eng. J. 203 (2012) 88–94.
[32] J. Wang, C. Ma, X. Mu, W. Cai, L. Liu, X. Zhou, W. Hu, Y. Hu, Construction of multifunctional MoSe2 hybrid towards the simultaneous improvements in fire safety and mechanical property of polymer, J. Hazard Mater. 352 (2018) 36–46.
[33] A. Patel, G. Coudurier, N. Essayem, C.V. Jacques, Effect of the addition of Sn to zirconia on the acidic properties of the sulfated mixed oxide, J. Chem. Soc. Faraday. Trans. 93 (1997) 347–353.
[34] A. Abdolahi, E. Hamzah, Z. Ibrahim, S. Hashim, Synthesis of uniform polyaniline nanofibers through interfacial polymerization, Materials 5 (2012) 1487–1494.
[35] Y. Hou, S. Qiu, Y. Hu, C.K. Kundu, Z. Gui, W. Hu, Construction of bimetallic ZIF-derived Co–Ni LDHs on the surfaces of GO or CNTs with a recyclable method: toward reduced toxicity of gaseous thermal decomposition products of unsaturated polyester resin, ACS Appl. Mater. Interfaces 10 (2018) 18359–18371.
[36] M.-S. Wu, C.-H. Yang, M.-J. Wang, Morphological and structural studies of nanoporous nickel oxide films fabricated by anodic electrochemical deposition techniques, Electrochim. Acta 54 (2008) 155–161.

[37] L. Ai, C. Zhang, L. Li, J. Jiang, Iron terephthalate metal–organic framework: revealing the effective activation of hydrogen peroxide for the degradation of organic dye under visible light irradiation, Appl. Catal. B Environ. 148–149 (2014) 191–200.
[38] M. Donohue, G. Aranovich, Classification of Gibbs adsorption isotherms, Adv. Colloid. Interfac. 76 (1998) 137–152.
[39] W.J. Zhou, S.Q. Song, W.Z. Li, Z.H. Zhou, G.Q. Sun, Q. Xin, S. Douvartzides, P. Tsiakaras, Direct ethanol fuel cells based on PtSn anodes: the effect of Sn content on the fuel cell performance, J. Power Sources 140 (2005) 50–58.
[40] Z. Sun, C. Cao, W.-Q. Han, A scalable formation of nano-SnO 2 anode derived from tin metal–organic frameworks for lithium-ion battery, RSC Adv. 5 (2015) 72825–72829.
[41] X. Zhou, Y. Yu, J. Yang, H. Wang, M. Jia, J. Tang, Cross-linking tin-based metal-organic frameworks with encapsulated silicon nanoparticles: high-performance anodes for lithium-ion batteries, ChemElectroChem 6 (2019) 2056–2063.
[42] X. Feng, W. Xing, L. Song, Y. Hu, In situ synthesis of a MoS2/CoOOH hybrid by a facile wet chemical method and the catalytic oxidation of CO in epoxy resin during decomposition, J. Mater. Chem. A. 2 (2014).
[43] W.J. Zhou, S.Q. Song, W.Z. Li, Z.H. Zhou, G.Q. Sun, Q. Xin, S. Douvartzides, P. Tsiakaras, Direct ethanol fuel cells based on PtSn anodes: the effect of Sn content on the fuel cell performance, J. Power Sources 140 (2005) 50–58.
[44] Y. Wang, A. Tabet-Aoul, M. Mohamedi, Room temperature synthesis of mixed platinum and tin oxide nanocomposite catalyst with enhanced mass activity and durability for ethanol electrooxidation in an acidic medium, J. Electrochem. Soc. 163 (2016) F1272–F1278.
[45] F. Chu, Y. Hou, L. Liu, S. Qiu, W. Cai, Z. Xu, L. Song, W. Hu, Hierarchical structure: an effective strategy to enhance the mechanical performance and fire safety of unsaturated polyester resin, ACS Appl. Mater. Interfaces 11 (2019) 29436–29447.
[46] M. Kim, C. Lee, J. Jang, Fabrication of highly flexible, scalable, and high-performance supercapacitors using polyaniline/reduced graphene oxide film with enhanced electrical conductivity and crystallinity, Adv. Funct. Mater. 24 (2014) 2489–2499.
[47] W. Cai, N. Hong, X. Feng, W. Zeng, Y. Shi, Y. Zhang, B. Wang, Y. Hu, A facile strategy to simultaneously exfoliate and functionalize boron nitride nanosheets via Lewis acid-base interaction, Chem. Eng. J. 330 (2017) 309–321.
[48] interfaces F. Liu, S. Luo, D. Liu, W. Chen, Y. Huang, L. Dong, L. Wang, Facile processing of free-standing polyaniline/SWCNT film as an integrated electrode for flexible supercapacitor application, ACS Appl. Mater. Interfaces 9 (2017) 33791–33801.
[49] Y. Xiao, Z. Jin, L. He, S. Ma, C. Wang, X. Mu, L. Song, Synthesis of a novel graphene conjugated covalent organic framework nanohybrid for enhancing the flame retardancy and mechanical properties of epoxy resins through synergistic effect, Compos. B Eng. 182 (2020) 107616.
[50] W. Hu, J. Zhan, N. Hong, T.R. Hull, A.A. Stec, L. Song, J. Wang, Y. Hu, Flame retardant polystyrene copolymers: preparation, thermal properties, and fire toxicities, Polym. Adv. Technol. 25 (2014) 631–637.
[51] S. Qiu, W. Hu, B. Yu, B. Yuan, Y. Zhu, S. Jiang, B. Wang, L. Song, Y. Hu, Effect of functionalized graphene oxide with organophosphorus oligomer on the thermal and mechanical properties and fire safety of polystyrene, Ind. Eng. Chem. Res. 54 (2015) 3309–3319.
[52] Y. Yuan, Y. Shi, B. Yu, J. Zhan, Y. Zhang, L. Song, C. Ma, Y. Hu, Facile synthesis of aluminum branched oligo (phenylphosphonate) submicro-particles with enhanced flame retardance and smoke toxicity suppression for epoxy resin composites, J. Hazard Mater. 381 (2020) 121233.
[53] B. Yu, W. Xing, W. Guo, S. Qiu, X. Wang, S. Lo, Y. Hu, Thermal exfoliation of hexagonal boron nitride for effective enhancements on thermal stability, flame retardancy and smoke suppression of epoxy resin nanocomposites via sol–gel process, J. Mater. Chem. A. 4 (2016) 7330–7340.
[54] S. Wang, B. Yu, K. Zhou, L. Yin, Y. Zhong, X. Ma, A novel phosphorus-containing MoS2 hybrid: towards improving the fire safety of epoxy resin, J. Colloid Interface Sci. 550 (2019) 210–219.
[55] J. Wang, J. Zhan, X. Mu, X. Jin, F. Chu, Y. Kan, W.J.J.o.c. Xing, i. science, Manganese phytate dotted polyaniline shell enwrapped carbon nanotube: towards the reinforcements in fire safety and mechanical property of polymer 529 (2018) 345–356.
[56] J.G. Wingkun, J.S. Knisely, S.H. Schnoll, G.R.J.P. Gutcher, Decreased carbon dioxide sensitivity in infants of substance-abusing mothers 95 (1995) 864–867.
[57] X. Qian, L. Song, Y. Hu, R.K.K. Yuen, Preparation and thermal properties of novel organic/inorganic network hybrid materials containing silicon and phosphate, J. Polym. Res. 19 (2012).
[58] J. Wang, D. Zhang, Y. Zhang, W. Cai, C. Yao, Y. Hu, W. Hu, Construction of multifunctional boron nitride nanosheet towards reducing toxic volatiles (CO and HCN) generation and fire hazard of thermoplastic polyurethane, J. Hazard Mater. 362 (2019) 482–494.
[59] X. Lu, F. Luo, Q. Xiong, H. Chi, H. Qin, Z. Ji, L. Tong, H. Pan, Sn-MOF derived bimodal-distributed SnO2 nanosphere as a high performance anode of sodium ion batteries with high gravimetric and volumetric capacities, Mater. Res. Bull. 99 (2018) 45–51.
[60] K. Yu, Z. Wu, Q. Zhao, B. Li, Y. Xie, High-temperature-stable Au@ SnO2 core/shell supported catalyst for CO oxidation, J. Phys. Chem. C 112 (2008) 2244–2247.
[61] W. Guo, B. Yu, Y. Yuan, L. Song, Y. Hu, In situ preparation of reduced graphene oxide/DOPO-based phosphonamidate hybrids towards high-performance epoxy nanocomposites, Compos. B Eng. 123 (2017) 154–164.
[62] R. Thomas, D. Yumei, H. Yuelong, Y. Le, P. Moldenaers, Y. Weimin, T. Czigany, S. Thomas, Miscibility, morphology, thermal, and mechanical properties of a DGEBA based epoxy resin toughened with a liquid rubber, Polymer 49 (2008) 278–294.
[63] M. Abdalla, D. Dean, D. Adibempe, E. Nyairo, P. Robinson, G. Thompson, The effect of interfacial chemistry on molecular mobility and morphology of multiwalled carbon nanotubes epoxy nanocomposite, Polymer 48 (2007) 5662–5670.